THE JOURNAL OF BIOLOGICAL CHEMISTRY VOL. 281, NO. 42, pp. 31689–31695, October 20, 2006

Crystallographic Analysis of Calcium-dependent Heparin Binding to Annexin A2*

Received for publication, May 10, 2006, and in revised form, July 26, 2006 Published, JBC Papers in Press, August 1, 2006, DOI 10.1074/jbc.M604502200

Chenghua Shao[‡], Fuming Zhang[§], Melissa M. Kemp[§], Robert J. Linhardt[§], David M. Waisman[¶], James F. Head[‡], and Barbara A. Seaton[‡1]

From the [‡]Department of Physiology and Biophysics, Boston University School of Medicine, Boston, Massachusetts 02118, the [§]Departments of Chemistry and Chemical Biology, Biology and Chemical and Biological Engineering, Rensselaer Polytechnic Institute, Troy, New York 12180, and the [¶]Department of Biochemistry and Molecular Biology, Dalhousie University, Halifax, Nova Scotia B3H 1X5, Canada

Annexin A2 and heparin bind to one another with high affinity and in a calcium-dependent manner, an interaction that may play a role in mediating fibrinolysis. In this study, three heparin-derived oligosaccharides of different lengths were co-crystallized with annexin A2 to elucidate the structural basis of the interaction. Crystal structures were obtained at high resolution for uncomplexed annexin A2 and three complexes of heparin oligosaccharides bound to annexin A2. The common heparin-binding site is situated at the convex face of domain IV of annexin A2. At this site, annexin A2 binds up to five sugar residues from the nonreducing end of the oligosaccharide. Unlike most heparin-binding consensus patterns, heparin binding at this site does not rely on arrays of basic residues; instead, main-chain and side-chain nitrogen atoms and two calcium ions play important roles in the binding. Especially significant is a novel calcium-binding site that forms upon heparin binding. Two sugar residues of the heparin derivatives provide oxygen ligands for this calcium ion. Comparison of all four structures shows that heparin binding does not elicit a significant conformational change in annexin A2. Finally, surface plasmon resonance measurements were made for binding interactions between annexin A2 and heparin polysaccharide in solution at pH 7.4 or 5.0. The combined data provide a clear basis for the calcium dependence of heparin binding to annexin A2.

Annexins are a family of Ca^{2+}-dependent membrane-binding eukaryotic proteins that have been implicated in a myriad of physiological processes, including membrane trafficking, cell signaling, ion transport, inflammation, apoptosis, and hemostasis (1). Most functional properties of annexins are attributed to their ability to bind membrane phospholipids and certain other anionic polymers, including glycosaminoglycans (GAGs)[2] such as heparin and heparan sulfate, in a Ca^{2+}-dependent manner.

Human annexin A2 is abundantly expressed in various tissues such as brain, spleen, kidney, lung, placenta, intestine, and the adrenal glands, and in intracellular and extracellular locations. Putative intracellular roles for annexin A2 include membrane trafficking and cytoskeletal actin bundling; and extracellular annexin A2 has been proposed to play a role in the fibrinolytic pathway (1). Annexin A2 often co-expresses with another protein, p11 (S100A10), forming an $(\text{annexin A2})_2$-$(\text{S100A10})_2$ heterotetramer (A2t). Monomeric and tetrameric annexin A2 share many of the same binding properties, *e.g.* the abilities to bind Ca^{2+}, phospholipid membranes, and certain GAGs (including heparin and heparan sulfate), albeit typically with some modification in affinity. The p11 component alone, despite belonging to the E-F hand family of Ca^{2+}-binding proteins, does not bind Ca^{2+} nor does it bind phospholipids or GAG. The association between annexin A2 and p11 does not require Ca^{2+} and utilizes the concave annexin molecular surface (2).

The putative role of annexin A2 in plasminogen activation through tissue plasminogen activator has been explored in previous studies (3, 4), as has the function of heparin in fibrinolysis (5, 6). The identification of annexin A2 as a heparin-binding protein (7) has raised the possibility that this protein-GAG interaction may participate in the regulation of thrombotic processes. To characterize the heparin-annexin A2 interaction and to determine the basis for its Ca^{2+} dependence, crystallographic studies were initiated on human annexin A2 in complex with heparin-derived oligosaccharides of varying lengths. Binding measurements in solution were also performed using surface plasmon resonance (SPR).

EXPERIMENTAL PROCEDURES

Annexin A2 Expression and Purification—Wild type human annexin A2 in vector pAED4.91 was transformed into *Escherichia coli* BL21 (DE3). Transformed cells were grown in LB Broth, Miller (American Bioanalytical). Cells were harvested by centrifugation at 6,000 × *g* for 15 min and resuspended in lysis

* This work was supported by National Institutes of Health Grants GM44554 (to B. S.), HL62244, and GM3806 (to R. J. L.). The costs of publication of this article were defrayed in part by the payment of page charges. This article must therefore be hereby marked "*advertisement*" in accordance with 18 U.S.C. Section 1734 solely to indicate this fact.

The atomic coordinates and structure factors (code 2HYU, 2HYV, 2HYW) have been deposited in the Protein Data Bank, Research Collaboratory for Structural Bioinformatics, Rutgers University, New Brunswick, NJ (http://www.rcsb.org/).

[1] To whom correspondence should be addressed: Dept. of Physiology and Biophysics, Boston University School of Medicine, 715 Albany St., Boston, MA 02118. Tel.: 617-638-5061; Fax: 617-638-4273; E-mail: seatonba@bu.edu.

[2] The abbreviations used are: GAGs, glycosaminoglycans; A2t, $(\text{annexin A2})_2$-$(\text{S100A10})_2$ heterotetramer; SPR, surface plasmon resonance; Δ^4UAp2S, 4-deoxy-α-L-*threo*-2-sulfo-hex-4-enopyranosyluronic acid; IdoAp2S, 2-*O*-sulfo-α-L-idopyranosyluronic acid; GlcNpS6S, 2-deoxy-,2-sulfamido, 6-*O*-sulfo-α-D-glucopyranose; r.m.s.d., root mean square deviation.

buffer containing 100 mM Tris, pH 7.5, 200 mM NaCl, 2 mM dithiothreitol, 1 mM EGTA, and protease inhibitors (Sigma), including 0.5 mM phenylmethylsulfonyl fluoride, 5 μg/ml pepstatin, 0.2 mM 4-(2-aminoethyl)benzenesulfonyl fluoride, 5 μg/ml aprotinin, 0.5 mM benzamidine, and 5 μM E-64. The cell solution was sonicated for 6 min and centrifuged at 100,000 × *g* for 1 h. The supernatant was precipitated with 50% $(NH_4)_2SO_4$ and centrifuged at 27,000 × *g* for 20 min. This supernatant was then applied to a butyl-Sepharose column (Amersham Biosciences), and annexin A2 was eluted with a linear gradient from 50 to 0% $(NH_4)_2SO_4$ in the lysis buffer. The fractions containing annexin A2 were then dialyzed against sample buffer (20 mM HEPES, pH 7.5, 100 mM NaCl, 1 mM EGTA, and 1 mM dithiothreitol). The dialyzed sample then was applied to a DEAE-Sepharose column (Amersham Biosciences). Pure annexin A2 protein was in the flow-through from the column. SDS-PAGE and matrix-assisted laser desorption ionization-mass spectrometry confirmed the presence of the intact full-length annexin A2 polypeptide.

Heparin-derived Oligosaccharide Isolation—Three oligosaccharides were co-crystallized with annexin A2 as follows: heparin-derived tetrasaccharide, hexasaccharide, and octasaccharide. Homogenous heparin oligosaccharides were purified as described previously (8).

Crystallographic Analysis—Crystals of annexin A2 in the absence of heparin were grown at 17 °C by vapor diffusion against a reservoir solution containing 14% PEG8000, 0.1 M Tris, pH 8.5, 10 mM $CaCl_2$, and 15% glycerol was added for cryo-protection. For the complexes, 10 mg/ml annexin A2 and 20 mM of each of three heparin-derived oligosaccharides were mixed and co-crystallized similarly by vapor diffusion at 17 °C against solutions containing 0.8–1.0 M 1,6-hexanediol, 0.1 M sodium acetate, pH 4.8–5.0, and 10–15 mM $CaCl_2$. Evaporation of the droplet provided sufficient cryo-protection from the concentrated mother liquor.

Crystallographic data from the tetrasaccharide-annexin A2 complex crystal was collected at the Brookhaven National Laboratory Synchrotron X8C beam-line. Data from the uncomplexed annexin A2 crystal, hexasaccharide-bound and octasaccharide-bound annexin A2 complex crystals were collected on an *R*-axis IV imaging plate detector mounted on a Rigaku RU-300 rotating anode generator. To collect high resolution data of the hexasaccharide-bound annexin A2 crystal, the 2θ angle was set at 10°. All crystals were directly cooled to 80–100 K by vapor nitrogen stream prior to collection. Data were indexed, integrated, and scaled using the DENZO and SCALEPACK software packages (9).

Phases were provided by molecular replacement using the program EPMR (10) and previous structures of annexin A2 (Protein Data Bank entry 1W7B) and annexin A5 (Protein Data Bank entry 1G5N) as starting models. Model building and refinement steps were carried out using O (11) and CNS (12), respectively. For the complexes, initial $F_o - F_c$ difference electron density maps provided the locations of the bound heparin saccharides, which were included in subsequent refinement using parameters employed previously (8). For all structures, individual *B*-factors were refined for all atoms. Data collection and refinement statistics of the crystallization work are presented in Table 1. Figures were all made through Pymol (13).

SPR Analysis of Annexin A2-Heparin Interactions—SPR measurements were performed on a BIAcore 3000 (BIAcore AB, Uppsala, Sweden) operated using the version software. Streptavidin sensor chip was from BIAcore. There is an average of one unsubstituted amino group within each heparin chain (14). This unsubstituted amino group was biotinylated as described previously (15). The resulting biotinylated heparin was then immobilized on the streptavidin chip based on the manufacturer's protocol. The successful immobilization of heparin was confirmed by the observation of an ~500 resonance unit increase in the sensor chip.

For the measurement of protein interactions with heparin, HBS-P buffer (0.01 M HEPES, 0.15 M NaCl, 0.005% polysorbate 20 (v/v), pH 7.4, from BIAcore) with the addition of 5 mM $CaCl_2$ was used as running buffer. Annexin A2 samples were diluted in HBS-P with Ca^{2+} and injected at a flow rate of 30 μl/min. At the end of each sample injection, the Ca^{2+}-free buffer was flowed over the sensor surface to facilitate dissociation. After a 3-min dissociation time, the sensor surface was regenerated by injecting with 30 μl of 2 M NaCl in 100 mM acetate buffer, pH 4.5. The response was monitored as a function of time (sensorgram) at 25 °C. The resulting sensorgrams were used for kinetic parameter determination by globally fitting to a 1:1 Langmuir binding model using BIAEvaluation software 4.0.1 (BIAcore AB, Uppsala, Sweden).

RESULTS

Annexin A2 Structure without Heparin Bound—The N-terminal 30 amino acids of the annexin A2 were not visible in the structure, leaving Asn^{31} as the first observed residue. Mass spectrometry run on the recovered crystal confirmed the absence, presumably due to proteolysis, of these residues (data not shown). The 2.10 Å structure of the uncomplexed annexin A2 is very similar to that of the human annexin A2 A66E mutant with seven Ca^{2+} bound (16) (Protein Data Bank entry 1XJL), main-chain r.m.s.d. of 0.617 Å and overall r.m.s.d. of 1.036 Å. Following the conserved annexin core domain model, the sequence from Asn^{31} to Asp^{338} is divided into four homologous repeats (I–IV), each constituting a structurally similar domain containing five α-helices. The entire molecular structure is that of a slightly curved disk with the four subdomains arranged in a near-parallel pattern. Seven Ca^{2+} are bound on the convex face of the protein (Fig. 1).

Annexin A2-Tetrasaccharide Complex—In this 1.86-Å resolution structure, a single tetrasaccharide is bound at the convex side of domain IV near the IV-AB and IV-DE loops (Fig. 2*A*). Clear electron density is observed for all sugar residues. The structure of annexin A2 in the tetrasaccharide-bound complex is very similar (main-chain r.m.s.d. of 0.529 Å and overall r.m.s.d. of 0.914 Å) to that of uncomplexed annexin A2, with only minor differences occurring in some loops (Fig. 1). This observation is consistent with previous studies (7). Residue A of Δ^4UAp2S at the nonreducing end is in the $^1H_2$ form. Subsequent residue B of GlcNpS6S is in the predominant $^4C_1$ conformation. The next residue of IdoAp2S adopts the $^1C_4$ chair form. The last residue, residue D of GlcNpS6S, is in the same conformation as that of residue B (Fig. 2).

TABLE 1
Crystallographic data and refinement statistics

	AN2[a]	AN2 + tetrasaccharide	AN2 + hexasaccharide
Diffraction data			
Resolution (Å)	2.10	1.86	1.42
Space group	$P2_1$	$P2_12_12$	$P2_12_12$
Unit cell			
a (Å)	60.5	107.9	107.7
b (Å)	64.3	54.3	54.3
c (Å)	104.2	68.9	68.6
β	91.73°	90.0°	90.0°
No. of reflections	45,423	32,153	75,286
Completeness[b] (%)	96.7 (93.6)	92.6 (94.8)	97.9 (83.5)
Redundancy	3.6	4.3	5.0
R_{merge}[c] (%)	6.7 (33.1)	7.5 (34.9)	5.5 (37.5)
Refinement			
Resolution range (Å)	40-2.10	50-1.86	50-1.42
R_{cryst}[d]	0.2142	0.1986	0.2118
R_{free}[e]	0.2563	0.2322	0.2227
No. of monomers in arbitrary units	2	1	1
No. of protein atoms	4956	2478	2478
No. of ions (Ca^{2+})	14	5	5
No. of heparin atoms	0	70	85
No. of water molecules	438	432	518
No. of atoms total	5408	2985	3086
R.m.s.d.[f] angles	1.0534°	0.9901°	1.0404°
R.m.s.d. bonds (Å)	0.0053	0.0046	0.0045
Mean $\langle B \rangle$ overall (Å^2)	30.1	20.8	22.3
Mean $\langle B \rangle$ protein (Å^2)	29.6	18.7	19.6
Mean $\langle B \rangle$ heparin (Å^2)		27.9	28.2
Ramachandran plot (%)[g]			
Most favored	93.7	94.7	94.7
Additional allowed	6.0	4.9	4.9
Generously allowed	0.4	0.0	0.0
Disallowed	0.0	0.4	0.4

[a] AN2 indicates annexin A2.
[b] Completeness is reported for all reflections and for the highest resolution shell (values in parentheses).
[c] R_{merge} reported for all reflections and for the highest resolution shell (values in parentheses); $R_{merge} = \Sigma|I_i - \langle I \rangle|/\Sigma I_i$, where I_i is the intensity of an individual reflection, and $\langle I \rangle$ is the mean intensity of that reflection.
[d] $R_{cryst} = \Sigma||F_p| - |F_{calc}||/\Sigma|F_p|$, where $|F_{calc}|$ and $|F_p|$ are the calculated and observed structure factors, respectively.
[e] R_{free} is defined as in Brünger *et al.* (12).
[f] r.m.s.d. indicates root mean square deviation.
[g] Data were calculated using Procheck (23). The sole residue in either generously allowed or disallowed regions corresponds to Val^{50} in the I-AB Ca^{2+}-binding loop.

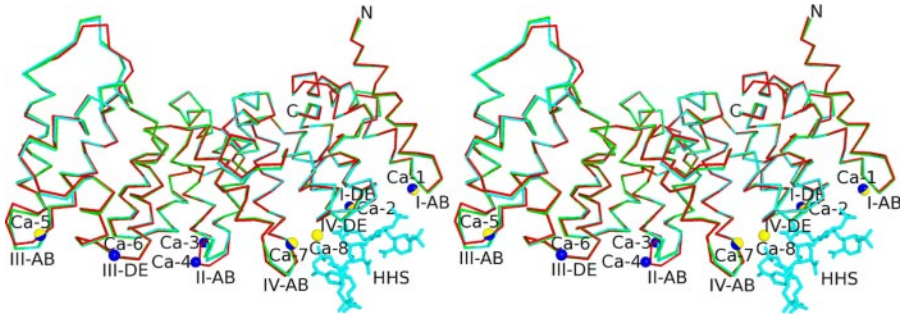

FIGURE 1. **Structural alignment (backbone representation) of annexin A2 structures; uncomplexed annexin A2 (*red*), tetrasaccharide-bound annexin A2 (*green*), and hexasaccharide-bound annexin A2 (*cyan*).** Structures are shown in wall-eyed stereo view. *Blue spheres* depict Ca^{2+} ions unique to the uncomplexed annexin A2 structure; *yellow spheres* indicate Ca-8; *blue/yellow spheres* indicate Ca^{2+} ions present in all structures. For clarity, only the oligosaccharides from the hexasaccharide complex (*cyan*, labeled as *HHS*) are shown.

In our studies, the residue at the nonreducing end (residue A) of each heparin oligosaccharide has been modified from IdoAp2S to Δ^4UAp2S. The modification introduces a double bond between C-4 and C-5, a result of heparin lyase digestion when the homogeneous oligosaccharide was generated (17). The modification appears unlikely to influence the binding of residue A to annexin A2. The binding interactions should be similar in Δ^4UAp2S and IdoAp2S because the interacting atoms are present in both residues. In addition, the ample space at the residue A-binding site and the flexible interactions with Lys^{280} could accommodate either a $^1C_4$ chair or $^2S_0$ skew boat conformation for IdoAp2S as well as the more constrained $^1H_2$ conformation observed for Δ^4UAp2S.

Five Ca^{2+} ions are observed in the crystal structure of the tetrasaccharide-annexin A2 complex (Fig. 1). Four occupy previously identified Ca^{2+}-binding sites, whereas the fifth binds at a Ca^{2+}-binding site that has not been observed in other annexin A2 structures (16, 18). This novel Ca^{2+}-binding site lies between the IV-AB and IV-DE loop, where it participates in heparin binding. The three Ca^{2+} ions found in the heparin-free annexin A2 structure but not in the annexin A2-tetrasaccharide complex correspond to the type II (or type AB) and type AB′ Ca^{2+}-binding sites at the II-AB loop and the type III (or type DE) Ca^{2+}-binding site at III-DE loop. In the absence of these Ca^{2+}, the II-AB loop adopts a significantly different conformation, and the Lys^{248} side chain in tetrasaccharide-bound annexin A2 occupies the site where Ca-6 is bound at the III-DE loop of the uncomplexed structure.

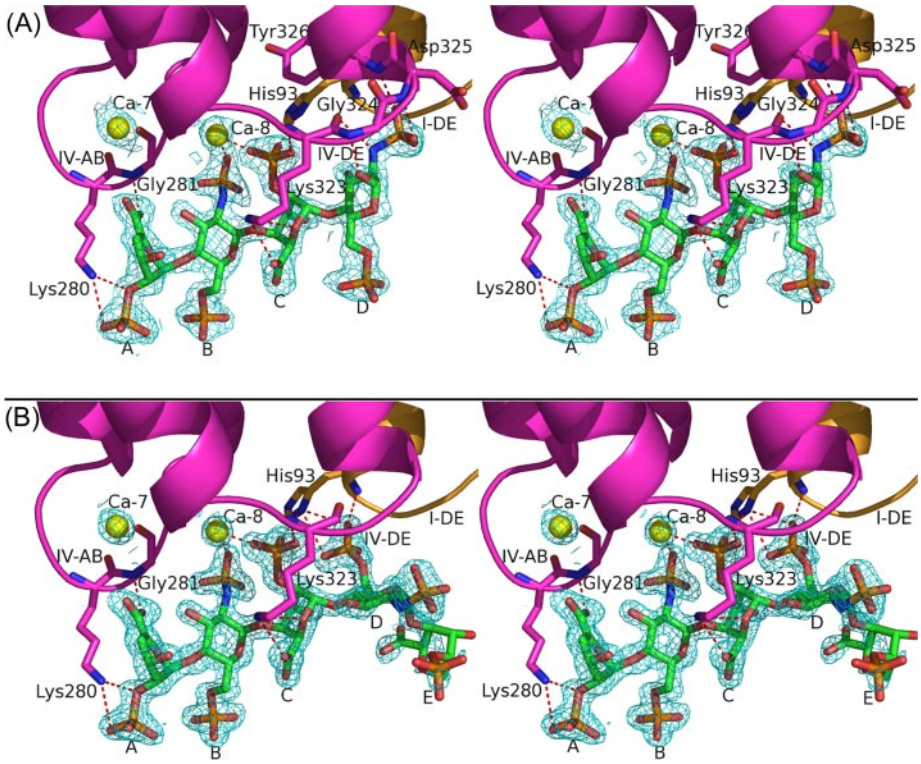

FIGURE 2. **Structures and electron density of the heparin tetrasaccharide (*A*) and hexasaccharide (*B*) bound to annexin A2.** Electron density, contoured at 1σ, is from simulated-annealing omit map omitting the oligosaccharides, Ca-7 and Ca-8. Structures are shown in wall-eyed stereo view. Domains I and IV are *colored orange* and *magenta*, respectively. *Yellow spheres* denote Ca^{2+}. *Red dashed lines* represent polar contacts between annexin A2 and oligosaccharides or Ca-8, as listed in Table 2. Heparin oligosaccharide residues from left (nonreducing end) to right are designated as: *A*, Δ^4UAp2S; *B*, GlcNpS6S; *C*, IdoAp2S; *D*, GlcNpS6S; *E*, IdoAp2S.

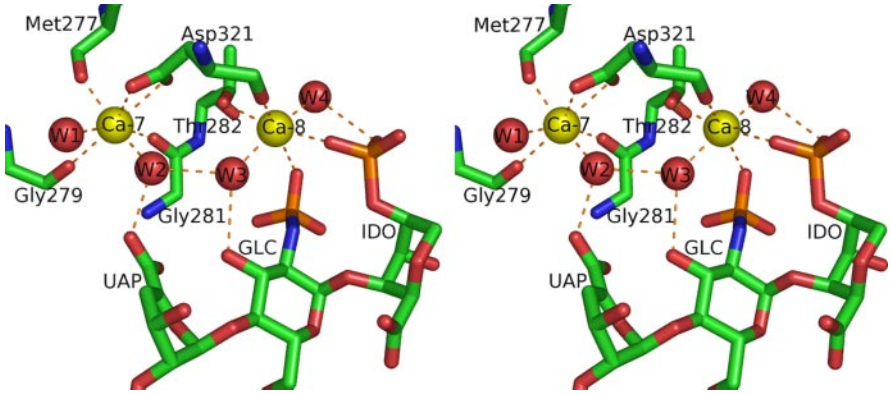

FIGURE 3. **Calcium coordination at the heparin-binding site.** Structure is displayed in wall-eyed stereo view. Ca^{2+} ions are shown as *yellow spheres* and water molecules as *red spheres. Orange dashed lines* denote Ca^{2+} coordination bonds and interactions between water molecules and oligosaccharide. All distances between Ca^{2+} ions and oxygen ligands fall between 2.3 and 2.6 Å.

Two of the five Ca^{2+} ions observed in the tetrasaccharide complex participate directly or indirectly in binding heparin (Figs. 2 and 3). Ca-7, which is also found in the IV-AB loop of uncomplexed annexin A2, does not interact directly with the tetrasaccharide but exhibits indirect interactions with the carboxyl group of tetrasaccharide residue A through a water molecule (Fig. 3). In contrast, the novel Ca^{2+} ion Ca-8 makes direct contact with the sulfate groups of residues B and C of the tetrasaccharide (Fig. 3 and Table 2). The coordination shell of Ca-8 includes two oxygen atoms from the sulfate groups of residues B and C, oxygen atoms from the Thr^{282} side chain and the Asp^{321} main chain, and two water molecules (Fig. 3). Ca-7 and Ca-8 are only 5.8 Å apart and are interlinked through two water molecules as well as Asp^{321}, which coordinates both Ca-7 and Ca-8 through side-chain and main-chain oxygen atoms, respectively.

In addition to the protein-bound Ca^{2+} ion, heparin interacts with annexin A2 through polar interactions, mostly between its sulfate oxygen atoms and the nitrogen atoms from the IV-AB (Gly^{279}–Arg^{283}) and IV-DE (Thr^{322}–Tyr^{326}, including the N-terminal end of helix E of domain IV) loop residues of annexin A2 (Fig. 2*A* and Table 2). The carboxylate group of tetrasaccharide residue A interacts with the main-chain nitrogen of Gly^{281} and the water network around Ca-7, whereas the oxygen atoms of the sulfoester and sulfate group make contact with the side-chain nitrogen of Lys^{280}. Tetrasaccharide residue B makes its sole contribution to the complex though complexation of Ca-8 via an *N*-sulfo oxygen. Similarly, residue C of tetrasaccharide coordinates Ca-8 via an *O*-sulfo oxygen. In addition, there are relatively weak electrostatic interactions between residue C and the His^{93} and Lys^{323}. For residue D, hydrogen bonds form between the tetrasaccharide ring and the *N*-sulfo oxygen and nitrogen atoms and the main-chain nitrogen atoms of Gly^{324}, Asp^{325}, and Tyr^{326}, locking the sugar residue into position.

Heparin adopts an extended conformation in solution (19). The dihedral angles (Φ, Ψ) for the GlcNpS6S(1→4)IdoAp2S and IdoAp2S(1→4)GlcNpS6S glycosidic linkages are around 80 and 110° and −70 and 120°, respectively (20). The dihedral angles observed in crystallographic or NMR structures can vary from these values by up to 50°. In the crystallographic tetrasaccharide-annexin A2 complex, the dihedral angles (defined as in Ref. 20) for the internal GlcNpS6S(1→4)IdoAp2S bond between residues B and C are 82 and 95°, close to the commonly observed values. However, the IdoAp2S(1→4)GlcNpS6S glycosidic linkage between residues C and D has dihedral angles of −110 and −61°, which is farther from the common values for this type of linkage.

TABLE 2

Polar contacts between heparin oligosaccharides and protein atoms or Ca-8

The first three heparin residues share the same interactions in both annexin A2-tetrasaccharide and annexin A2-hexasaccharide complexes, and given distances represent averages between the two structures; interactions for residue D differ in the two complexes.

Heparin type	Heparin residue	Heparin atom	Protein atom/calcium ion	Distance
				Å
	A (Δ^4UAp2S)	O-2 (sulfoester)	Lys^{280}(N-ζ)	3.2
		O-22 (sulfate)	Lys^{280}(N-ζ)	3.4
		O-7 (carboxylate)	Gly^{281}(N)	2.8
Tetrasaccharide/hexasaccharide	B (GlcNpS6S)	O-22 (sulfate)	Ca-8	2.5
		O-22 (sulfate)	Ca-8	2.4
		O-23 (sulfate)	His^{93}(N-δ1)	3.4
	C (IdoAp2S)	O-24 (sulfate)	Lys^{323}(N)	3.0
		O-5 (ring)	Lys^{323}(N-ζ)	3.4
		O-7 (carboxylate)	Lys^{323}(N-ζ)	3.1
Tetrasaccharide	D (GlcNpS6S)	O-1 (ring)	Gly^{324}(N)	2.9
		O-22 (sulfate)	Tyr^{326}(N)	2.8
		O-22 (sulfate)	Asp^{325}(N)	3.2
		O-24 (sulfate)	Asp^{325}(N)	2.9
		N (sulfamide)	Lys^{323}(O)	3.4
		O-62 (sulfate)	His^{93}(N-δ1)	3.2
Hexasaccharide	D (GlcNpS6S)	O-64 (sulfate)	His^{93}(N-δ1)	3.1
		O-64 (sulfate)	His^{93}(N)	3.0

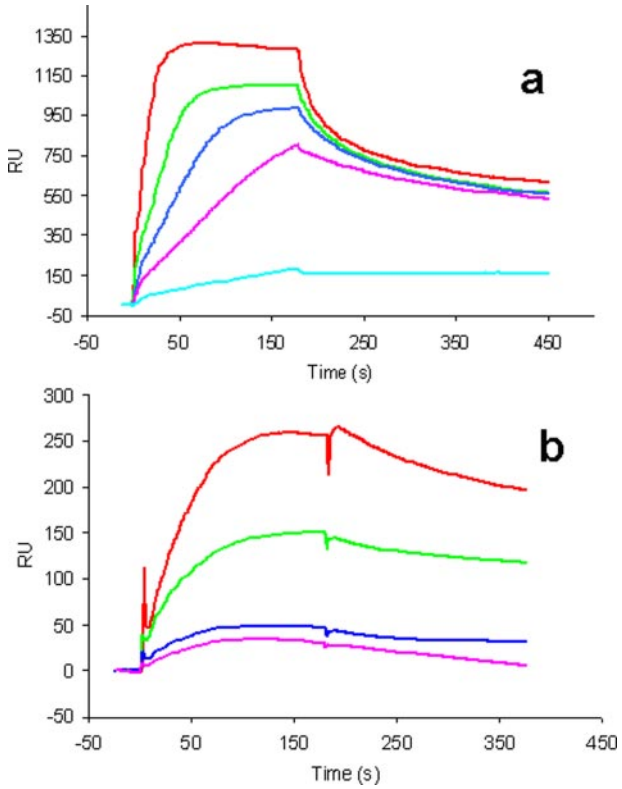

FIGURE 4. **SPR analysis of the annexin A2 interaction with heparin polysaccharide.** *a*, sensorgrams of annexin A2-heparin interaction at pH 7.4. Annexin A2 concentrations (from *top* to *bottom*): 500, 200, 100, 50, and 10 nM. *b*, sensorgrams of annexin A2-heparin interaction at pH 5.0. Annexin A2 concentrations (from *top* to *bottom*): 4000, 2000, 1000, and 500 nM.

TABLE 3

SPR kinetic measurements of annexin A2 interactions with heparin polysaccharide in the presence of 5 mM $CaCl_2$

pH	k_{on} (1/M·s)	k_{off} (1/s)	K_d (M)
7.4	7.93×10^5	0.0133	1.68×10^{-8}
5.0	2.45×10^3	8.89×10^{-4}	3.66×10^{-7}

Annexin A2-Hexasaccharide Complex—The crystal structure of the annexin A2-hexasaccharide complex at 1.42 Å, the highest resolution among all published annexin crystal structures, is similar (overall r.m.s.d. of 0.241 Å) to that of annexin A2-tetrasaccharide (Fig. 1). Electron density is observed for the first four sugar residues and only for part of the fifth residue on the convex side of domain IV of annexin A2 (Fig. 2*B*). There is no observed electron density for the sixth hexasaccharide residue. Comparison of the two complexes (annexin A2-tetrasaccharide and annexin A2-hexasaccharide) shows that the first three residues (A, B, and C) of the hexasaccharide are in the same position, conformation, and orientation as the first three residues of the tetrasaccharide, but the fourth residue (D) differs in the two structures (Fig. 2 and Table 2). In the annexin A2-tetrasaccharide complex, the *N*-sulfo group of residue D binds to annexin A2 through IV-DE loop residues. Residue D in the annexin A2-hexasaccharide complex is still in the $^4C_1$ conformation; however, it is rotated by 135° around the 1→4 linkage between residues C and D. In the latter orientation, hydrogen bonds or salt bridges are formed between the *O*-sulfo oxygen atoms of residue D and main-chain and side-chain nitrogen atoms of His^{93} from the I-DE loop. With this orientation of residue D, the dihedral angles of the C-D glycosidic linkage are −120 and 83°, close to the commonly observed values for the IdoAp2S(1→4)GlcNpS6S linkage (20). Moreover, residue D of the tetrasaccharide binds exclusively to the IV-DE loop, whereas residue D of the hexasaccharide interacts solely with the neighboring I-DE loop (Table 2). Residue E of the hexasaccharide shows no direct binding to any protein atoms or bound Ca^{2+} ions; the only mutual interactions are through water molecules.

The annexin A2-octasaccharide complex is very similar (overall r.m.s.d. of 0.24 Å) to that of annexin A2-hexasaccharide. Despite its greater length, the octasaccharide makes the same interactions involving the first five sugar residues, and the electron density is weaker for the fifth than for the first four sugars. In both of these longer complexes, residues beyond the first five do not interact observably with the protein and lack clear electron density. Because of its substantial similarity to the

hexasaccharide complex, the octasaccharide complex is not discussed further herein.

Kinetic Measurements of Protein Interactions with Heparin—Because crystals of the annexin A2-heparin complexes are grown under mildly acidic pH conditions, the binding properties of annexin A2 to full-length heparin at this pH were investigated using SPR. Solution measurements were made at pH 5.0 and 7.4, with or without Ca^{2+} added (Fig. 4). The results confirm that in the absence of Ca^{2+}, annexin A2 exhibits no binding to the heparin chip at either pH 7.4 or pH 5.0 (data not shown), whereas in the presence of 5 mM Ca^{2+}, strong binding is observed at both pH values. Table 3 shows the kinetics data calculated for the binding between full-length heparin and annexin A2. The binding affinity is lower at pH 5.0 than at pH 7.4 (calculated K_d values of 366 and 17 nM, respectively).

DISCUSSION

Dozens of heparin-binding proteins have been identified to date, but of these only a handful exhibit Ca^{2+}-dependent binding to heparin as follows: serum amyloid P component, P- and L-selectins, and annexin A5, a homolog of annexin A2 (17). Within this small subgroup, only annexin A5 (8) and annexin A2 (this study) have been studied as crystallographic ternary complexes with Ca^{2+} and heparin oligosaccharides. The crystallographic data reveal that Ca^{2+}-dependent heparin binding can arise from the following: 1) Ca^{2+}-dependent protein conformational changes that produce a favorable heparin-binding site (*indirect mechanism*), and/or 2) protein-Ca^{2+}-heparin ternary complex formation (*direct mechanism*). Both mechanisms are evident in the annexin A2-heparin oligosaccharide complexes. The indirect mechanism is exemplified by the stabilization of the IV-AB loop through coordination of Ca-7. Combined evidence from various crystallographic and spectroscopic studies indicates that Ca^{2+} coordination within annexin type II (or type AB) sites substantially stabilizes the loop conformations. In all four of the annexin A2 crystal structures, the IV-AB loop conformations are stabilized by Ca-7 coordination, independent of the presence or absence of heparin oligosaccharide. Thus the IV-AB loop conformation stabilized by Ca-7 offers a pre-formed binding surface suitable for oligosaccharide residue A. In contrast, the coordination of Ca-8 only occurs upon ternary complex formation, in which Ca-8 is a direct participant.

The motif of a primary, strong Ca^{2+} site serving as a nucleus for a second, weaker Ca^{2+} site that achieves full occupancy only as part of a ternary complex with another ligand has been noted previously for annexin A5 (21). In the present annexin A2 studies, the Ca-7 ion is coordinated similarly in the binary and ternary complexes, *i.e.* through five protein oxygen ligands and two solvent water molecules (Fig. 3). Ca-8, on the other hand, exhibits fewer contacts with the protein; the metal ion coordination is through two oxygen ligands from the protein, two sulfate oxygens from oligosaccharide residues B and C, and two water molecules. The two Ca^{2+} sites are interconnected through shared interactions with two water molecules and Asp^{321}. Such interlinked Ca^{2+} sites have been observed in other proteins besides annexins, *e.g.* pulmonary collectins (22).

The crystal structure of annexin A5 in complex with Ca^{2+} and heparin tetrasaccharide (8) shows a Ca^{2+}-dependent mode of oligosaccharide binding that is very similar to the indirect mechanism observed in annexin A2. In the annexin A5 ternary complex, the oligosaccharide does not coordinate the protein-bound Ca^{2+} but instead binds solely to protein atoms residing in a conformationally sensitive I-AB Ca^{2+}-binding loop. The Ca^{2+}-independent annexin A5-oligosaccharide binary complex occurring on the concave surface of that protein is not observed in the annexin A2 crystal structures. Heparin-binding sites at this location may be precluded in annexin A2 as a consequence of A2t heterotetramer formation, which involves the concave protein surface.

The modes of heparin oligosaccharide binding in all three annexin A2 complexes show common features that may be important for heparin polysaccharide recognition by the protein. In all complexes, the nonreducing end of the oligosaccharide binds at the IV-AB loop, consistent with a possible physiological recognition site for the nonreducing end of the free heparin polymer or the heparan sulfate GAG chain attached to a proteoglycan. However, IdoAp2S, the native counterpart of Δ^4UAp2S, should bind equally well here and can occupy either terminal or internal positions throughout the GAG chains. The crystallographic data therefore suggest that either the IV-AB site inherently prefers the GAG nonreducing end or that the modification on residue A somehow enhances binding affinity at the IV-AB loop in the crystallographic complexes. In addition, despite differences in oligosaccharide length, the first three sugar residues bind with virtually identical conformations at the same site on the protein. Only the fourth residue in the tetrasaccharide has different conformation from that of the corresponding residue D in the longer oligosaccharides. The conformational difference may be imposed by its shorter length of the tetrasaccharide and the resulting hydrogen bond with the nitrogen atom of Gly^{324} via the free O-1 hydroxyl group within the residue D sugar ring (Fig. 2*A* and Table 2). With the longer heparin oligosaccharides, the O-1 oxygen of residue D is not in the free hydroxyl form but forms the 1→4 glycosidic linkage to residue E rather than making contact with the protein. In both of the longer oligosaccharides, the fifth residue is less clear in electron density, suggestive of flexibility and weaker binding, and subsequent residues (6th-8th) are not observed at all. Thus, comparison of the three complex structures suggests that the first 4–5 residues (from the nonreducing end) are critical for heparin recognition and binding and that the corresponding sugar residues in a naturally occurring heparin polysaccharide are more likely to adopt the conformations seen in the longer oligosaccharides.

The present work offers a structural basis for several previously reported observations related to the binding in solution of heparin polysaccharides to A2t (7). First, the previous solution study reports that the binding interaction shows Ca^{2+} dependence and requires a minimum of 4–5 monosaccharides. The crystallographic data are consistent with these results; all three oligosaccharides bind strongly to annexin A2 via the same four sugar residues (A–D) and exhibit weaker binding for a fifth in the longer oligosaccharides. The SPR data confirm that no detectable binding of A2 to the

heparin-immobilized chip occurs in the absence of Ca^{2+}. In addition, the binding constants for A2 and A2t at neutral pH, despite different measurement techniques (SPR for A2 and circular dichroism for A2t), are comparable, 17 and ~30 nM, respectively. The SPR kinetic data best fit a 1:1 stoichiometry (*i.e.* one heparin polysaccharide per one annexin A2 molecule), consistent with the crystallographic data that reveal a single oligosaccharide-binding site on the protein. The combined data from the two studies therefore suggest that the heparin-binding site seen in the crystallographic complexes represents the primary, major site of heparin interaction in both annexin A2 and A2t. The two studies are also in agreement regarding conformational differences related to heparin binding by annexin A2 or A2t. The crystallographic and CD data concur in finding that heparin binding induces no significant conformational change in annexin A2 alone. However, it is notable that a heparin-induced conformational transition occurs in A2t that can be observed in CD spectra (7). This observation suggests that heparin interacts in some way with the annexin-bound p11 molecule and/or the protein-protein complex to induce a structural transition in A2t. The CD data also reveal that a smaller, heparin-induced, Ca^{2+}-independent conformational change occurs in A2t. This study further proposed that A2t-specific transitions may involve a polybasic stretch of sequence in domain IV near the concave surface of the annexin A2 component, perhaps in conjunction with p11 residues.

In summary, this study provides evidence that annexin A2 exhibits significant Ca^{2+}-dependent heparin-binding properties either as a monomeric protein or as a component of the A2t heterotetramer. These properties derive primarily from a single heparin-binding site formed by two Ca^{2+}-binding loops located at the convex side of domain IV that binds 4–5 saccharide residues from the nonreducing end. The characterized features of this site provide a structural basis for specific, Ca^{2+}-dependent recognition of heparin polysaccharides by annexin A2.

REFERENCES

1. Gerke, V., Creutz, C. E., and Moss, S. E. (2005) *Nat. Rev. Mol. Cell Biol.* **6,** 449–461
2. Waisman, D. M. (1995) *Mol. Cell. Biochem.* **149**, 301–322
3. Kang, H. M., Choi, K. S., Kassam, G., Fitzpatrick, S. L., Kwon, M., and Waisman, D. M. (1999) *Trends Cardiovasc. Med.* **9,** 92–102
4. Hajjar, K. A., and Acharya, S. S. (2000) *Ann. N. Y. Acad. Sci.* **902,** 265–271
5. Liang, J. F., Li, Y., and Yang, V. C. (2000) *Thromb. Res.* **97,** 349–358
6. Bell, J., Duhon, S., and Doctor, V. M. (2003) *Blood Coagul. Fibrinolysis* **14,** 229–234
7. Kassam, G., Manro, A., Braat, C. E., Louie, P., Fitzpatrick, S. L., and Waisman, D. M. (1997) *J. Biol. Chem.* **272,** 15093–15100
8. Capila, I., Hernaiz, M. J., Mo, Y. D., Mealy, T. R., Campos, B., Dedman, J. R., Linhardt, R. J., and Seaton, B. A. (2001) *Structure* (*Camb.*) **9,** 57–64
9. Otwinowksi, Z., and Minor, W. (1997) *Methods Enzymol.* **27,** 307–326
10. Kissinger, C. R., Gehlhaar, D. K., and Fogel, D. B. (1999) *Acta Crystallogr. Sect. D Biol. Crystallogr.* **55,** 484–491
11. Jones, T. A., Zou, J. Y., Cowan, S. W., and Kjelgaard, M. (1991) *Acta Crystallogr. Sect. D Biol. Crystallogr.* **47,** 110–119
12. Brünger, A. T., Adams, P. D., Clore, G. M., DeLano, W. L., Gros, P., Grosse-Kunstleve, R. W., Jiang, J. S., Kuszewski, J., Nilges, M., Pannu, N. S., Read, R. J., Rice, L. M., Simonson, T., and Warren, G. L. (1998) *Acta Crystallogr. Sect. D Biol. Crystallogr.* **54,** 905–921
13. DeLano, W. L. (2002) *The PyMOL Molecular Graphics System*, DeLano Scientific, San Carlos, CA
14. Toida, T., Yoshida, H., Toyoda, H., Koshiishi, I., Imanari, T., Hileman, R. E., Fromm, J. R., and Linhardt, R. J. (1997) *Biochem. J.* **322,** 499–506
15. Hernaiz, M., Liu, J., Rosenberg, R. D., and Linhardt, R. J. (2000) *Biochem. Biophys. Res. Commun.* **276,** 292–297
16. Rosengarth, A., and Luecke, H. (2004) *Annexins* **1,** 129–136
17. Capila, I., and Linhardt, R. J. (2002) *Angew. Chem. Int. Ed. Engl.* **41,** 391–412
18. Burger, A., Berendes, R., Liemann, S., Benz, J., Hofmann, A., Gottig, P., Huber, R., Gerke, V., Thiel, C., Romisch, J., and Weber, K. (1996) *J. Mol. Biol.* **257,** 839–847
19. Mulloy, B., Forster, M. J., Jones, C., and Davies, D. B. (1993) *Biochem. J.* **293,** 849–858
20. Mulloy, B., and Forster, M. J. (2000) *Glycobiology* **10,** 1147–1156
21. Swairjo, M. A., Concha, N. O., Kaetzel, M. A., Dedman, J. R., and Seaton, B. A. (1995) *Nat. Struct. Biol.* **2,** 968–974
22. Hakansson, K., and Reid, K. B. (2000) *Protein Sci.* **9,** 1607–1617
23. Laskowski, R. A., MacArthur, M. W., Moss, D. S., and Thornton, J. M. (1993) *J. Appl. Crystallogr.* **26,** 283–291